JACS
JOURNAL OF THE AMERICAN CHEMICAL SOCIETY

ARTICLE

pubs.acs.org/JACS

Topotactic Transformations of Superstructures: From Thin Films to Two-Dimensional Networks to Nested Two-Dimensional Networks

Chuan Fei Guo,[†,§] Sihai Cao,[‡] Jianming Zhang,[†,§] Haoying Tang,[†,§] Shengming Guo,[†] Ye Tian,[†,§] and Qian Liu[†,§,⊥]

[†]National Center for Nanoscience and Technology, China, No. 11 Beiyitiao, Zhongguancun, Beijing 100190, China

[§]Graduate School of the Chinese Academy of Sciences, Beijing 100190, China

[‡]Beijing BOE Energy Technology Co., Ltd., No. 10 Jiuxianqiao Road, Beijing 100015, China

[⊥]TEDA Applied Physics School, Nankai University, Tianjin 300457, China

Supporting Information

ABSTRACT: Design and synthesis of super-nanostructures is one of the key and prominent topics in nanotechnology. Here we propose a novel methodology for synthesizing complex hierarchical superstructures using sacrificial templates composed of ordered two-dimensional (2D) nanostructures through lattice-directed topotactic transformations. The fabricated superstructures are nested 2D orthogonal Bi_2S_3 networks composed of nanorods. Further investigation indicates that the lattice matching between the product and sacrificial template is the dominant mechanism for the formation of the superstructures, which agrees well with the simulation results based on an anisotropic nucleation and growth analysis. Our approach may provide a promising way toward a lattice-directed nonlithographic nanofabrication technique for making functional porous nanoarchitectures and electronic devices.

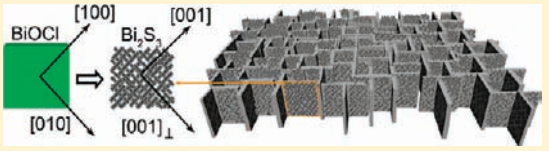

Hierarchical nanostructures have attracted increasing attention in recent years owing to their potential in constructing novel nanoarchitectures and nanodevices. Up to now, representative hierarchical building blocks are branched nanostructures, such as PbS/PbSe pine trees,[1−3] networks of SnO nanoribbons,[4] branched In_2O_3 nanowires,[5] and ZnO nanobridges and nanopropellers.[6,7] These branched structures are often synthesized using vapor phase deposition based on a series of sequential formations of one-dimensional (1D) nanostructures, for example, 1D nanowires,[1−9] or a two-step process by combining vapor-phase and hydrothermal techniques.[10] In most cases of such 1D formations, the branches are formed *on the surface* of preformed nanostructures via a "bottom-up" growth method.[1−10]

Compared with the 1D nanostructures, two-dimensional (2D) nanostructures are much easier to tailor to complex nanoarchitectures. Similar to the Chinese traditional papercut, a 2D "sacrificial" nanostructure (e.g., a nanoplate) could be "engraved" into specific hierarchical nanostructures by an *in situ* topotactic transformation in a 2D formation process. In such toptactic transformation, the morphologies of the hierarchical structures are mainly determined by the lattice structure, shape, and scale of the templates. Recently, Li et al. claimed successful synthesis of 2D Bi_2S_3 networks composed of single-crystalline Bi_2S_3 nanorods in a topotactic transformation process,[11] in which the BiOCl nanodiscs were used as the sacrificial template of Bi_2S_3 nanorods. However, the disk-like Bi_2S_3 networks were disordered because in their case the preformed BiOCl nanodiscs were crystallographically independent of each other and deposited randomly on the substrate. In comparison, ordered nanostructures are more desirable to fulfill preferable functions or construct specific architectures.[12] It is expected that using ordered or superstructured 2D sacrificial templates should be an effective way for synthesizing ordered hierarchical nanostructures or superstructures. To realize this purpose often requires a multistep process, in which the nanostructure formed in the early step (intermediate) acts as the template for the next step. To summarize, three essential conditions are needed to achieve ordered or superstructured hierarchical nanostructures: (1) a multistep process in which intermediates act as templates for the final products; (2) templates that are ordered structures or superstructures; (3) templates that are composed of 2D structures. How to obtain desired templates out of a suitable material system becomes one of the key issues.

Bismuth and its compounds are hot materials in the fields of thermoelectrics,[13,14] superconductors,[15] photocatalysts,[16,17] gas sensors,[18] electrochemical hydrogen storage and topological insulators,[11,19−21] etc. Among bismuth compounds, BiOCl, Bi_2O_3, and Bi_2S_3 are important semiconductors and their nanostructures are attracting considerable interest in recent years. BiOCl has a tetragonal structure with lattice parameters a = 3.887 Å and c = 7.354 Å and is often used as an excellent photocatalyst.[16,17] Tetragonal β-Bi_2O_3 is a metastable phase with a = 7.741 Å and c = 5.634 Å and is a promising material for oxygen sensors. Bi_2S_3 has an orthorhombic structure with a = 11.14 Å, b = 11.30 Å, and c = 3.981 Å, and is useful in the

Received: December 7, 2010
Published: March 23, 2011

applications of gas sensing, electrochemical hydrogen storage, and photovoltaics.[18,19,22] Layer-structured bismuth compounds are very common so that there are many structures with special disk- or sheet-like morphologies. The layered morphologies and structural transformations among different bismuth compounds may provide a way to synthesize complex hierarchical nanostructures.

In this paper, for the first time to our best knowledge, we report on the controllable synthesis of 2D orthogonal networks (2DONWs) of BiOCl nanowalls, as well as nested 2DONWs (N2DONWs) of Bi_2S_3 nanorods, via topotactic transformation processes. Here the superstructured BiOCl is used as the sacrificial template of the Bi_2S_3 N2DONWs. Epitaxial relationships among β-Bi_2O_3, BiOCl, and Bi_2S_3 are found to be the key to the formation of the superstructures. Because the raw material is an amorphous BiO_x thin film prepared by magnetron sputtering, the resulting super-nanostructures have a good uniformity and can be scaled-up for mass production.

SYNTHESIS AND FORMATION MECHANISM OF BiOCl 2DONWs

Amorphous BiO_x films with a typical thickness of 200 nm were first deposited on wafer substrates by magnetron sputtering and then heated at 500 °C to transform to β-Bi_2O_3 films (see Supporting Information Figure S1), which acted as the precursor of the subsequent nanostructures of BiOCl. During the crystallization of the amorphous layer, many crystalline domains in different crystal orientations were formed with an average diameter of ~25 μm. BiOCl nanowall networks were simply obtained by dipping the β-Bi_2O_3 films into diluted hydrochloric solution (concentration 0.24 M) for minutes.

Figure 1a is an optical micrograph of a BiOCl film composed of domains in different colors, which represent different morphologies. The 2DONWs shown in the scanning electron microscopy (SEM) images of Figure 1b (see also Supporting Information Figure S2) are made up of two sets of perpendicularly aligned BiOCl nanowalls with a typical length of 300 nm, height of 300 nm, and thickness of ~20 nm. The inset is a fast Fourier transform (FFT) pattern of the SEM image, clearly demonstrating that two sets of nanowalls are aligned perpendicularly. Note that not all nanowalls grow vertically to the substrate; some nanowalls are tilted or tiled, as displayed in Figure 1c. It has been verified that only the turquoise domains in Figure 1a are vertically aligned 2DONWs like that in Figure 1b, while the purple and yellow domains are tilted and tiled 2DONWs, respectively. The transmission electron microscopy (TEM) image and selected area electron diffraction (SAED) pattern in Figure 1d (corresponding amorphous BiO_x is 75 nm in order that the BiOCl 2DONWs are transparent under the exposure of electron beam) clearly show that each set of nanowalls are preferentially grown along the ⟨110⟩ direction and perpendicular to the [001] direction. The high-resolution (HR) TEM analysis in Figure 1e also gives the same result; and corresponding SAED pattern shows a lattice rotation within ±7°, which may be ascribed to the steric clash of the nanowalls in the growth process. The electron micrographs demonstrate that the 2DONW is a superstructure similar to a superlattice film, which implies that it may grow epitaxially from the β-Bi_2O_3 film. The epitaxial relationship can be further studied using TEM analysis.

Note that both β-Bi_2O_3 (d_{220} = 2.737 Å) and BiOCl (d_{110} = 2.751 Å) have tetragonal structures, and $d_{220|\beta} \approx d_{110|BiOCl}$ with a lattice mismatch f = 0.50% (in reference to β-Bi_2O_3). Also, the

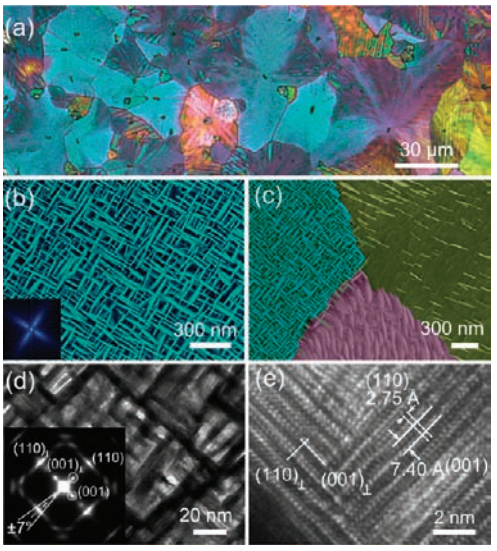

Figure 1. (a) Optical image of a BiOCl film, showing that the film is composed of many domains in different colors. (b) SEM image of a vertically grown 2DONW, inset is the corresponding FFT pattern. (c) SEM image of 2DONWs with three typical morphologies. (d) Bright field TEM image of a 2DONW. Inset is the corresponding SAED pattern, revealing that two sets of nanowalls are perpendicularly aligned with a lattice rotation within ±7°. (e) Corresponding HRTEM image.

$(002)_\beta$ facet with a spacing of 2.817 Å should also be considered. The equivalent $(220)_\beta$ and $(2\bar{2}0)_\beta$, as well as the $(002)_\beta$ facets, are with an approximate spacing and perpendicular to each other. By analyzing the crystal structures of β-Bi_2O_3 and BiOCl, we can predict two possible epitaxial relationships of β-Bi_2O_3 and BiOCl nanowalls:

(1) If two sets of nanowalls do not have an equivalent epitaxial relationship with β-Bi_2O_3, a possibility is $(110)_{BiOCl} \| (220)_\beta$, $(1\bar{1}0)_{BiOCl} \| (2\bar{2}0)_\beta$, and $[001]_{BiOCl} \| [001]_\beta$ for one set of nanowalls and $(110)_{BiOCl\perp} \| (002)_\beta$, $(1\bar{1}0)_{BiOCl\perp} \| (2\bar{2}0)_\beta$, and $[001]_{BiOCl\perp} \| [110]_\beta$ for the other set of nanowalls in the perpendicular direction (indicated by ⊥). In brief, two sets of BiOCl nanowalls are grown perpendicularly to the c- and [110]-axes of β-Bi_2O_3, respectively.

(2) If two sets of nanowalls have an equivalent epitaxial relationship with β-Bi_2O_3, they should grow from the β-Bi_2O_3 with the following crystallographic relationships: $(110)_{BiOCl} \| (220)_\beta$, $(1\bar{1}0)_{BiOCl} \| (002)_\beta$, $[001]_{BiOCl} \| [110]_\beta$; and $(110)_{BiOCl\perp} \| (2\bar{2}0)_\beta$, $(1\bar{1}0)_{BiOCl\perp} \| (002)_\beta$, $[001]_{BiOCl\perp} \| [1\bar{1}0]_\beta$. Or two sets of BiOCl nanowalls are grown perpendicularly to the [110]- and $[1\bar{1}0]$-axes of β-Bi_2O_3, respectively.

Comparing the above possibilities, the system in prediction 2 is relatively unstable because the lattice mismatch between the $\{002\}_\beta$ and $\{110\}_{BiOCl}$ is larger (f = 2.4%) so that the amount of misfit dislocations will increase by 65.7% compared with prediction 1, implying higher elastic energy density of dislocations. The elastic energy of dislocations per unit area, E_{ed}, can be estimated by[23]

$$E_{ed} \approx \frac{fYb}{8\pi(1-\nu^2)}\left(\ln\frac{r}{b}+1\right) \quad (1)$$

where b is the value of Burgers vector, r is the radius of the stress field of dislocations, and Y and ν are the Young's modulus and

dx.doi.org/10.1021/ja111000m | J. Am. Chem. Soc. 2011, 133, 8211–8215

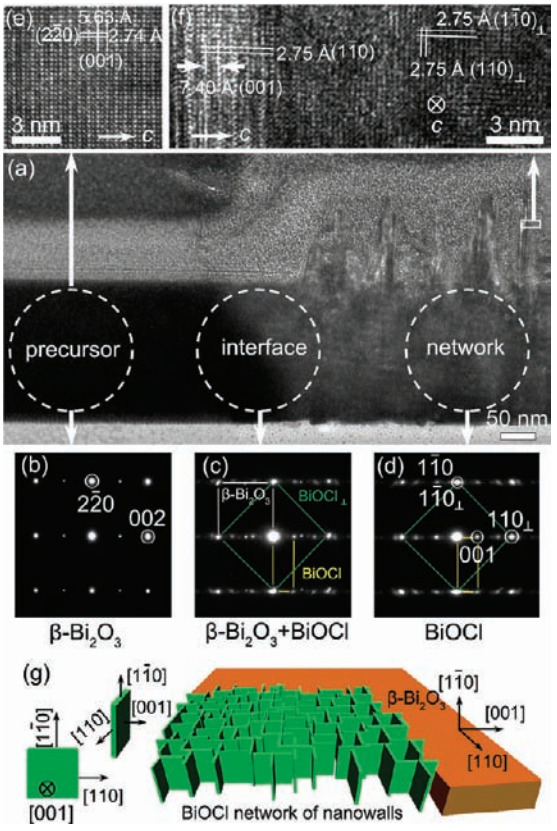

Figure 2. (a) Bright field TEM image of the slice obtained by FIB milling, only the right part of which has been dipped in HCl solution and transforms to a BiOCl 2DONW. The walls aligned perpendicularly to the electron beam are invisible because they are very thin but visible in the HRTEM image shown in panel f. (b–d) SAED patterns of the precursor (β-Bi_2O_3), interface, and formed BiOCl network, revealing that the BiOCl network grows epitaxially from β-Bi_2O_3. (e) HRTEM image of the β-Bi_2O_3 film. (f) HRTEM image of two perpendicularly aligned nanowalls. (g) A schematic illustration of a BiOCl 2DONW, clearly displaying the structural relationship of the BiOCl 2DONW and β-Bi_2O_3.

Poisson's ratio of BiOCl, respectively. According to eq 1, prediction 2 will result in an increase of elastic energy of dislocation of at least 19.1% compared with that in predication 1 (because $r \leq b/(2f)$). Hence, we argue that prediction 1 is more reasonable.

In order to confirm the actual structural relationship between the β-Bi_2O_3 precursor and the BiOCl 2DONW, a TEM study of a heterostructured BiOCl/Bi_2O_3 slice obtained by focused ion beam (FIB) milling was carried out. In the TEM observation, the electron beam was along the [001] zone axis of a set of BiOCl nanowalls (and the [110] direction of the other set). Figure 2a is a bright field TEM image of the slice. The HRTEM image and SAED patterns in Figure 2b–f indicate that the BiOCl grows epitaxially from Bi_2O_3, with the relationships of $(1\bar{1}0)_{BiOCl} \| (2\bar{2}0)_\beta$ and $(001)_{BiOCl} \| (001)_\beta$; $(1\bar{1}0)_{BiOCl\perp} \| (2\bar{2}0)_\beta$ and $(110)_{BiOCl\perp} \| (002)_\beta$. Therefore, the above-mentioned prediction 1 agrees well with the experimental results. It can be concluded that two sets of perpendicularly woven nanowalls from the top view can be observed only when both the *c*- and [110]-axes of the β-Bi_2O_3 parallel the film plane.

There also exist single crystalline β-Bi_2O_3 domains whose *c*- and [110]-axes are not parallel to the film plane. In this case,

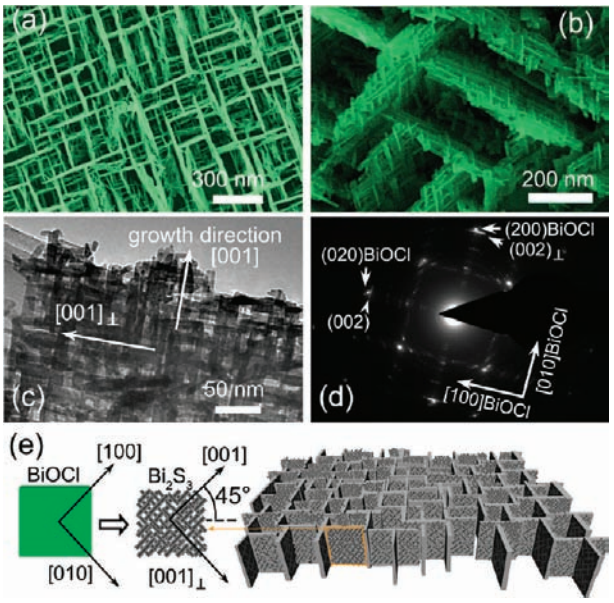

Figure 3. (a) SEM image of a Bi_2S_3 N2DONW. (b) Tilt view of a N2DONW in high magnification, showing that each nanowall has evolved to a 2D network made up of nanorods. (c) Bright field TEM image of a Bi_2S_3 network, which is composed of two sets of perpendicularly woven nanorods. (d) Corresponding SAED pattern indicates that all Bi_2S_3 nanorods are along the ⟨001⟩ fast growth direction and grown epitaxially from the BiOCl nanowall. (e) A model of the Bi_2S_3 N2DONW, displaying the structural relationship of Bi_2S_3 and BiOCl.

the formed BiOCl 2DONWs are tilted (see Figure 1c). If the tilted angle approximates to 90° or the *c*-axis is perpendicular to the film plane, only a few vertically aligned walls are observed, while most of the walls are tiled on the substrate (see the yellow part of Figure 1c and Supporting Information Figure S3).

The wall-like morphology of BiOCl could be ascribed to the layered growth of BiOCl. BiOCl is composed of many five-layer-stacked Cl–Bi–O–Bi–Cl monolayers or "macromolecules" bonded with each other by the van der Waals force, which results in strongly anisotropic growth. As a matter of fact, the fast growth is in the *c*-plane, similar to graphite.[24,25] Therefore, BiOCl prefers to grow to layered structures with a high aspect ratio. In addition, the lattice spacing of the {110} facets of BiOCl (2.751 Å) is very close to those of the {220} and {002} facets of β-Bi_2O_3 (2.737 and 2.817 Å, respectively). Therefore, it should be the epitaxial and layered growth of BiOCl on single-crystalline β-Bi_2O_3 that leads to the formation of the special morphology of 2DONWs. Finally, the fact that a metastable β-phase can be eroded by acids is also a prerequisite for the formation of BiOCl 2DONWs.

SYNTHESIS AND FORMATION MECHANISM OF Bi_2S_3 N2DONWs

The superstructured BiOCl 2DONW is an ideal template for making more complex hierarchical superstructures. First, the BiOCl 2DONW is a superstructure itself. Second, it is composed of quasi-2D nanowalls. Third, a BiOCl nanowall is a single crystal so that it has potential to transform to other crystalline nanostructures in a lattice-matching directed process. Actually, it has been recently shown that a BiOCl 2D nanostructure can transform to a superstructured network of Bi_2S_3 nanorods by reacting with a preblended solution of thioacetamide (TAA) and

hydrochloric acid at 60 °C for tens of hours.[11] Bi_2S_3 is an extremely insoluble substance with a solubility product K_{sp} down to 1×10^{-97}; the insoluble BiOCl can still transform to Bi_2S_3 with the presence of S^{2-}. Therefore, if a β-Bi_2O_3 film is put into preblended solution of TAA and hydrochloric acid, in the first step, BiOCl 2DONWs will be formed at once (because BiOCl 2DONWS can be formed in minutes), and in the next step, each nanowall can act as the template for the formation of Bi_2S_3 network. The building blocks that construct the Bi_2S_3 2DONW are 2DONWs themselves, so that the Bi_2S_3 nanostructure here is a self-similar structure: a nested 2D orthogonal network (N2DONW) composed of Bi_2S_3 nanorods. This has been conducted in our experiments (see Supporting Information). The N2DONW is very interesting because it is a self-similar superstructure and also an ideal morphology for gas sensing, photocatalytical activities, electrochemical hydrogen storage, as well as a desirable nanostructure for constructing complex architectures. Moreover, the *in situ* synthesis of the N2DONWs from amorphous films guarantees good uniformity on a large scale.

Figure 3a−c illustrates Bi_2S_3 N2DONWs transformed from BiOCl 2DONWs. The Bi_2S_3 N2DONW maintains the original profile of the BiOCl 2DONW but each nanowall has evolved to a network or a fence-like structure composed of nanorods. The rods with an average diameter of ~15 nm are aligned along the ⟨100⟩ directions of the original BiOCl nanowall template, as indicated in the SAED pattern in Figure 3d. The ⟨001⟩ directions are the common fast growth directions of Bi_2S_3 nanostructures.[26,27] However, a nanorod has no definite crystallographic orientation in reference to the BiOCl nanowall precursor besides $\langle 001\rangle_{Bi_2S_3} \| \langle 100\rangle_{BiOCl}$ (see Figure S4). Crystallographic-preferential growth of Bi_2S_3 is the reason that the nanorods are ordered and perpendicularly woven. That is, the Bi_2S_3 grows on BiOCl with (001) (spacing 3.890 Å) parallel to the (100) and (010) facets (spacing 3.981 Å) of BiOCl. Since BiOCl possesses a tetragonal structure, an orthogonal morphology of Bi_2S_3 network is reasonable. And according to the lattice matching, the nanorods have a ~45° angle in reference to the intersecting lines of two nanowalls, as shown in Figure 3b,e.

The textured growth of Bi_2S_3 is related to its crystal structure. Bi_2S_3 has an orthorhombic structure with a = 11.14 Å, b = 11.30 Å, and c = 3.981 Å. The a and also b planes interact by van de Waals force,[27] so that the growth in both a- and b-directions is limited. As a result, Bi_2S_3 often presents a c-axis fast growth direction and rod-like structures. The lattice matching between the c-plane of Bi_2S_3 and {100} planes of BiOCl gives rise to the [001] oriented growth of Bi_2S_3 nanorods in two equivalent and perpendicular directions from a sacrificial template of the BiOCl nanowall. While many hierarchical nanostructures based on epitaxy or lattice matching can be obtained,[1−10] there are few examples that ordered 2D templates are used to construct highly complex hierarchical superstructures in combination of topotactic transformations. In our work, several crystal phases (including the β-Bi_2O_3 precursor, intermediate BiOCl superstructure, and targeted Bi_2S_3 superstructure) and phase transformations (from a β-Bi_2O_3 domain to a BiOCl 2DONW composed of nanowalls, and from a BiOCl nanowall to a Bi_2S_3 2DONW composed of nanorods) are involved in the fabrication process. Each phase transformation is facilitated by the relationships of morphology and crystal structure, resulting eventually in targeted complex nanostructures (i.e., Bi_2S_3 N2DONWs) as a whole.

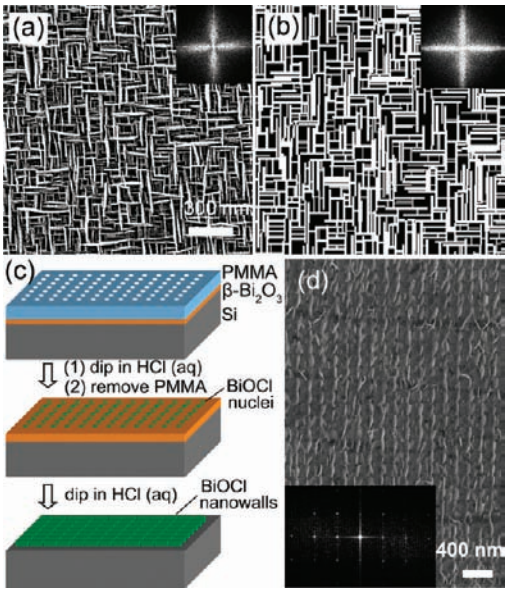

Figure 4. (a) SEM image and (b) simulation result of a 2DONW. The corresponding FFT patterns indicate that the 2DONW is not a periodic structure. (c) Schematic illustration of the fabrication of a BiOCl nanowall array with periodic configuration by introducing an artificial nuclei array. (d) SEM image of a BiOCl nanowall array in a periodic structure; corresponding FFT pattern indicates that it is a nanowall lattice. The c-axis of the β-Bi_2O_3 film is tilted with its projection line along the growth direction of the nanowalls.

LATTICE-DIRECTED NANOFABRICATION AT HIGH THROUGHPUT

The formation of the 2DONWs and N2DONWs includes two processes: nucleation and growth. Take the BiOCl 2DONWs for example: BiOCl nuclei are first epitaxially formed on the surface of a β-Bi_2O_3 film with the presence of H^+ and Cl^-(aq), then they will grow accompanied with the formation and growth of new nuclei. The nuclei are oriented in two perpendicular directions (i.e., [110] and [001] directions of β-Bi_2O_3). Nucleation and growth stop when the β-Bi_2O_3 film is consumed completely. This analysis is very similar to the nucleation and growth processes in a classical phase change. However, anisotropic nucleation and growth should be considered. We used MATLAB to simulate the growth process. In the simulation, we presume that the nucleation rate is constant and growth rate of ⟨110⟩ direction is 15 times that of the ⟨001⟩ direction, the nuclei are formed on random locations of a β-Bi_2O_3 film whose c- and [110]-axes are parallel to the film plane. Simulation results agree well with our experimental morphology, as shown in Figure 4a,b. It also proves that our structural analysis is reasonable. The Bi_2S_3 2DONWs are formed in a very similar but much slower process.

Although the BiOCl nanowalls are orthogonally woven, the pitch between two neighboring nanowalls is indeterminate (indicated by the FFT pattern of Figure 4a,b) because the locations of nuclei are random. To fabricate uniform and periodic BiOCl nanowalls, we should first fabricate a periodic BiOCl nucleus array. For this purpose, we spin-coated a polymethyl methacrylate (PMMA) layer on a β-Bi_2O_3 film and obtained a periodic pattern (orthogonal hole array with diameter of 30 nm and pitch of 200 nm) by e-beam lithography, then dipped the specimen in HCl solution (see Figure 4c) so that a BiOCl nucleus array was formed. After removing the PMMA film, the exposed

β-Bi_2O_3 film with a periodic BiOCl array was put into HCl solution again. In this case, it should be easier for Bi^{3+} to diffuse to the preformed nuclei than to form new nuclei. Therefore, the preformed periodic nuclei grew to nanowalls, leading to a periodically aligned BiOCl nanowall array, or nanowall lattice, as shown in the SEM image in Figure 4d. The corresponding FFT pattern indicates the nanowall lattice is indeed a periodic structure.

We have provided a simple and cost-effective way of fabricating specific hollowed-out nanostructures without the use of lithography. The formation process of N2DONWs combines both top-down and bottom-up methods directed by lattice matching among different phases. Compared with the mainstream nanofabrication techniques, it is more effective to build superstructures on large area with the size of the building blocks (i.e., nanowalls and nanorods) down to 10−20 nm at least in one dimension. Thus, our work may provide a new methodology for constructing complex hierarchical nanostructures with lattice ordering. Also we have proven that these nanostructures can be fabricated in designable configurations such as periodic pattern.

In summary, we have demonstrated a methodology that combines both top-down and bottom-up processes for synthesizing complex hierarchical nanostructures, exemplified by 2D orthogonal networks of BiOCl 2D nanowalls, as well as nested 2D orthogonal networks of Bi_2S_3 nanorods, for the first time. Structural analysis revealed that the special morphological evolution of the hierarchical nanostructures is directed by the crystallographic lattice matching: in the formation of a BiOCl 2DONW, two sets of BiOCl nanowalls grow perpendicularly to the *c*- and [110]-axes of β-Bi_2O_3, respectively; and in the evolution from a BiOCl 2DONW to a Bi_2S_3 N2DONW, the [001]-oriented Bi_2S_3 nanorods grows along the [100] and [010] directions of each BiOCl nanowall. Prospectively, such hierarchical nanostructures hold great potential in constructing novel nanodevices. Our work provides a way toward lattice-directed nonlithographic nanofabrications with specific hollowed-out nanoarchitectures at high throughput and low cost. Following this demonstration, opportunities in designing and fabricating even more complex and interesting hierarchical superstructures based on bismuth compounds or other layered material systems are possible.

■ ASSOCIATED CONTENT

Ⓢ Supporting Information. An experimental section describing the synthesis of materials, preparation of TEM specimen, and characterization of nanostructures, together with an XRD result of a β-Bi_2O_3 film and detailed structural analysis of the formation of the Bi_2S_3 nanorod network from a BiOCl nanoplate. This material is available free of charge via the Internet at http://pubs.acs.org.

■ AUTHOR INFORMATION

Corresponding Author
liuq@nanoctr.cn; guoshengming@nanoctr.cn

■ ACKNOWLEDGMENT

This work is supported by NSFC (Grant 10974037), NBRPC (Grant 2010CB934102), and International S&T Cooperation Program (Grant 2010DFA51970). The authors thank Dr. X. Qi at NCNST for providing convenience in using TEM and K. Peng for the preparation of TEM specimen using FIB. C. F. Guo thanks Prof. L.-M. Qi for useful discussion.

■ REFERENCES

(1) Bierman, M. J.; Lau, Y. K. A.; Kvit, A. V.; Schmitt, A. L.; Jin, S. *Science* **2008**, *320*, 1060–1063.
(2) Lau, Y. K. A.; Chernak, D. J.; Bierman, M. J.; Jin, S. *J. Am. Chem. Soc.* **2009**, *131*, 16461–16471.
(3) Zhu, J.; Peng, H.; Marshall, A. F.; Barnett, D. M.; Nix, W. D.; Cui, Y. *Nat. Nanotechnol.* **2008**, *3*, 477–481.
(4) Wang, Z. L.; Pan, Z. *Adv. Mater.* **2002**, *14*, 1029–1032.
(5) Wan, Q.; Dattoli, E. N.; Fung, W. Y.; Guo, W.; Chen, Y.; Pan, X.; Lu, W. *Nano Lett.* **2006**, *6*, 2909–2915.
(6) Lao, J. Y.; Huang, J. Y.; Wang, D. Z.; Ren, Z. F. *Nano Lett.* **2003**, *3*, 235–238.
(7) Gao, P. X.; Wang, Z. L. *Appl. Phys. Lett.* **2004**, *84*, 2883–2885.
(8) Fan, H. J.; Scholz, R.; Kolb, F. M.; Zacharias, M. *Appl. Phys. Lett.* **2004**, *85*, 4142–4144.
(9) Guo, C. F.; Wang, Y.; Jiang, P.; Cao, S.; Miao, J.; Zhang, Z.; Liu, Q. *Nanotechnology* **2008**, *19*, No. 445710.
(10) Cheng, C.; Liu, B.; Yang, H.; Zhou, W.; Sun, L.; Chen, R.; Yu, S. F.; Zhang, J.; Gong, H.; Sun, H.; Fan, H. J. *ACS Nano* **2009**, *3*, 3069–3076.
(11) Li, L.; Sun, N.; Huang, Y.; Qin, Y.; Zhao, N.; Gao, J.; Li, M.; Zhou, H.; Qi, L. *Adv. Funct. Mater.* **2008**, *18*, 1194–1201.
(12) Xu, S.; Shen, Y.; Ding, Y.; Wang, Z. L. *Adv. Funct. Mater.* **2010**, *20*, 1493–1497.
(13) Venkatasubramanian, R.; Siivola, E.; Colpitts, T.; O'Quinn, B. *Nature* **2001**, *413*, 597–602.
(14) Heremans, J.; Thrush, C. M. *Phys. Rev. B* **1999**, *59*, 12579–12583.
(15) Parendo, K. A.; Tan, K. H. S. B.; Goldman, A. M. *Phys. Rev. B* **2007**, *76*, No. 100508(R).
(16) Chai, S. Y.; Kima, Y. J.; Jung, M. H.; Chakraborty, A. K.; Jung, D.; Lee, W. I. *J. Catal.* **2009**, *262*, 144–149.
(17) Deng, Z.; Chen, D.; Peng, B.; Tang, F. *Cryst. Growth Des.* **2008**, *8*, 2995–3303.
(18) Yao, K.; Gong, W. W.; Hu, Y. F.; Liang, X. L.; Chen, Q.; Peng, L.-M. *J. Phys. Chem. C* **2008**, *112*, 8721–8724.
(19) Li, L.; Cao, R.; Wang, Z.; Li, J.; Qi, L. *J. Phys. Chem. C* **2009**, *113*, 18075–18081.
(20) Chen, Y. L.; Analytis, J. G.; Chu, J.-H.; Liu, Z. K.; Mo, S.-K.; Qi, X. L.; Zhang, H. J.; Lu, D. H.; Dai, X.; Fang, Z.; Zhang, S. C.; Fisher, I. R.; Hussain, Z.; Shen, Z.-X. *Science* **2009**, *325*, 178–181.
(21) Zhang, H.; Liu, C.-X.; Qi, X.-L.; Dai, X.; Fang, Z.; Zhang, S.-C. *Nat. Phys.* **2009**, *5*, 438–442.
(22) Liu, Z.; Peng, S.; Xie, Q.; Hu, Z.; Yang, Y.; Zhang, S.; Qian, Y. *Adv. Mater.* **2003**, *15*, 936–940.
(23) Tu, K.-N.; Mayer, J. W.; Feldman, L. C. *Electronic Thin Film Science: For Electrical Engineers and Materials Scientists*; Macmillan: New York, 1992.
(24) Cao, S.; Guo, C.; Lv, Y.; Guo, Y.; Liu, Q. *Nanotechnology* **2009**, *20*, No. 257502.
(25) Peng, H. L.; Chan, C. K.; Meister, S.; Zhang, X. F.; Cui, Y. *Chem. Mater.* **2009**, *21*, 247–252.
(26) Koh, Y. W.; Lai, C. S.; Du, A. Y.; Tiekink, E. R. T.; Loh, K. P. *Chem. Mater.* **2003**, *15*, 4544–4554.
(27) Sigman, M. B., Jr; Korgel, B. A. *Chem. Mater.* **2005**, *17*, 1655–1660.